Università degli studi di Padova
Dipartimento di Fisica e Astronomia "GALILEO GALILEI"

Corso di Laurea in Fisica
Tesi di Laurea

Asimmetrie nella distribuzione dei tempi di decadimento dei mesoni B_s^0 ricostruiti nei canali $D_s^*\pi$ e D_s^*K

B_s^0 folded time asymmetry studies in the $D_s^*\pi$ and D_s^*K decay modes

Laureando:
Samuele Cavinato
Matricola:
1100007

Relatore:
Dott. Alessandro Bertolin

Anno Accademico 2016 - 2017

Contents

Chapter 1

Introduction

The work presented in the following pages focuses on the so-called flavour-tagging at the LHCb experiment. The LHCb detector, operated at the LHC [4, 5], is a single-arm forward spectrometer covering the pseudorapidity range $2 < \eta < 3$, designed for precision measurements of CP violation and rare decays of beauty and charm hadrons. In this work the following decays of the B_s^0 mesons are considered:

$$B_s^0 \to D_s^{*-}\pi^+$$
$$B_s^0 \to D_s^{*\mp}K^\pm$$

where additionally:

$$\begin{aligned} D_s^{*-} &\to D_s^- \ \gamma \\ D_s^- &\to K^+K^-\pi^- \\ D_s^- &\to K^-\pi^+\pi^- \\ D_s^- &\to \pi^+\pi^-\pi^- \end{aligned}$$

The particle which accompaines the final state D_s^* meson is called "bachelor-particle". In the specific decay channels described, it can be a charged *pion* or a charged *kaon*.
In Figures 1.1a and 1.1b the invariant masses of the B_s^0, in the $D_s^{*\mp}K^\pm$ decay channel, and the $D_s^{*\mp}$ mesons are shown, respectively. The data set used corresponds to an integrated luminosity of about 3 fb^{-1} collected in the 2011-2012 data taking period.

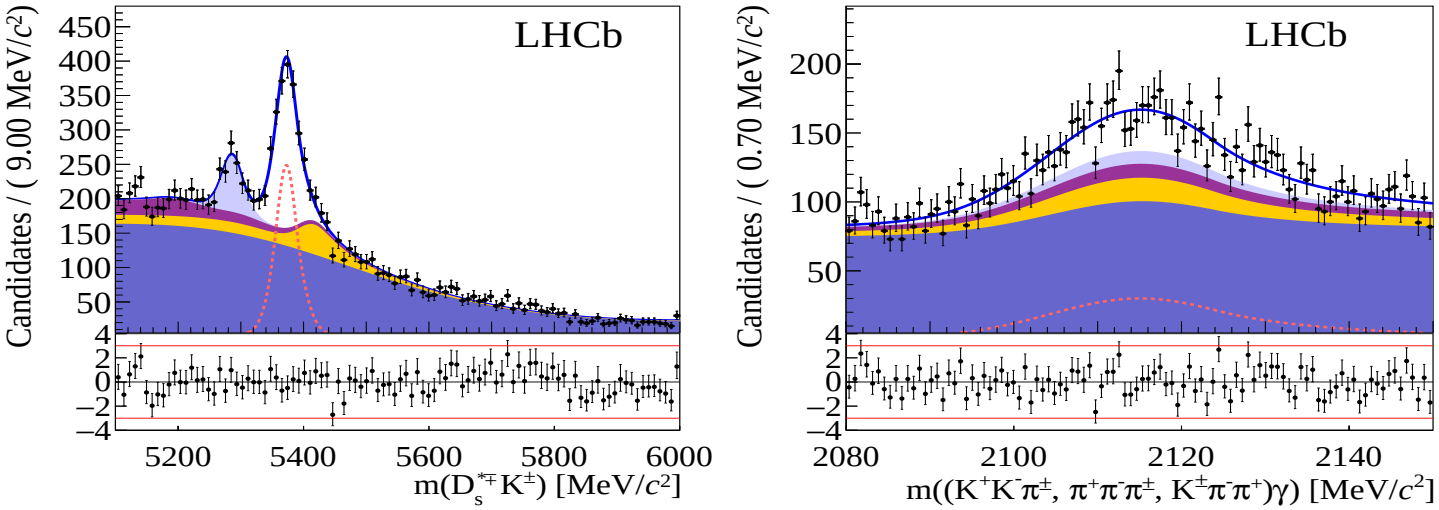

(a) **(b)**

Figure 1.1: Figure (a) shows the invariant mass of the B_s^0 meson in the $D_s^{*\mp}K^\pm$ decay channel; Figure (b) shows the invariant masses of the $D_s^{*\mp}$ mesons in three different decay cannels.

The measurement of CP violation is related to the weak phase γ [7, 8], one of the least well-determined CKM matrix parameters. γ can be measured using time-dependent studies of the $B_s^0 \to D_s^{*\mp} K^{\pm}$ decays [9].
The observables of this decay can be related to those of $B^0 \to D^{*-}\pi^+$ and $B_s^0 \to D_s^{*-}\pi^+$, opening the possibility of a combined extraction of γ. The ratio $\mathcal{R} \equiv \mathcal{B}\,(B_s^0 \to D_s^{\mp} K^{\pm})/\mathcal{B}\,(B_s^0 \to D_s^{-}\pi^+)$ is predicted to be $\mathcal{R} = 0.0086^{+0.009}_{-0.007}$ and it has been measured by LHCb [6] to be $\mathcal{R} = 0.0762 \pm 0.0015 \pm 0.0020$, where the first uncertainty is statistical and the second systematic. Under the same theoretical assumpion, the ratio $\mathcal{R}^* \equiv \mathcal{B}\,(B_s^0 \to D_s^{*\mp} K^{\pm})/\mathcal{B}\,(B_s^0 \to D_s^{*-}\pi^+)$ is predicted to be $\mathcal{R}^* = 0.099 \pm 0.0030 \pm 0.0036$. It has recently been measured for the very first time by the LHCb collaboration [3] to be $\mathcal{R}^* = 0.068 \pm 0.005\ ^{+0.003}_{-0.002}$.
In the following Chapters several studies concerning these specific decay channels will be shown. In Chapter 2 two different flavour-tagging algorithms and the standard way to combine them will be described. In Chapter 3 the calibration of the three algorithms, using $B_s^0 \to D_s^{*-}\pi^+$ MonteCarlo[1] data, will be checked. The average mistag fraction and the tagging efficiency of each algoritmh will be calculated. In Chapter 4 time asymmety studies made on the two decay channels will be presented and some consideration on CP violation will be done.

[1] In the following MC will be use instead of MonteCarlo.

Chapter 2

Flavour-tagging

2.1 General information

Precision measurement of flavour-oscillation of B_s^0 mesons and of the CP asymmetries in their decays allow the validity of the standard model of particle physics to be probed at energy scales non directly accessible by current colliders.
The analisys of the collected data requires the so-called flavour tagging algorithms [2] to identify the flavour at production of the reconstructed B meson. So, it's extremely important to test the effectivness of these algorithms on the brand new decay mode considered.
There are many different flavour-tagging algorithms, but they can be divided in two main different types:

- **Opposite-side (OS) algorithms:** they exploit the fact that b quarks are predominantly produced in $b\bar{b}$ pairs in hadron collision and thus the flavour at production of the reconstructed B meson is opposite to that of the oher b hadron in the event. Therefore, the products of the decay chain of the other b hadron in the event can be used for flavour tagging.
- **Same-side (SS) algorithms**[1]**:** they look for particles produced in association with the reconstructed B meson in the hadronisation process. In about 50% of cases a B_s^0 meson is accompained by a charged kaon. The charge of the latter particle indicates the b quark content of the B meson.

The effectivness of a tagging algorithm is quantified by the tagging efficiency, ϵ_{tag}, and the mistag fraction, ω. These variables are defined as:

$$\epsilon_{tag} = \frac{R+W}{R+W+U} \tag{2.1}$$

and

$$\omega = \frac{W}{W+R} \tag{2.2}$$

where R, W and U are the number of correctly tagged, uncorrectly tagged and untagged B candidates, respectively. These quantities are early accessible using simulated (MC) signal events. For each B candidate i, the flavour-tagging algorithm estimates the probability, η_i, of an incorrect tag decision. To correct for potential biases in η_i, a function $\omega(\eta)$ is used to calibrate the mistag probability to provide an unbiased estimate of the mistag fraction for any value of η. More detailes about the calibration of the algorithms used in this work will be presented later.

2.2 The combined SS+OS flavour-tagging algorithm

Generally, information from OS and SS algorithms can be combined during the analysys in order to perform a better tagging of the selected events. The LHCb standard procedure [1] to combine tagging

[1] In the following the Opposite-side and Same-side algorithms will be called OS and SS respectively

algorithms is described below.
The combined probability $P(b)$ that the meson contains a $b-$quark is calculated as

$$P(b) = \frac{p(b)}{p(b) + p(\bar{b})} \qquad P(\bar{b}) = 1 - P(b) \tag{2.3}$$

where

$$p(b) = \prod_i \left(\frac{1 + d_i}{2} - d_i(1 - \eta_i) \right) \qquad p(\bar{b}) = \prod_i \left(\frac{1 - d_i}{2} + d_i(1 - \eta_i) \right). \tag{2.4}$$

Here, d_i is the decision taken by the $i-$th tagger and η_i the corresponding predicted mistag probability. The combined decision and the corresponding mistag probability are d = -1 and η = 1 - $P(b)$ if $P(b) > P(\bar{b})$, otherwise d = +1 and η = 1 - $P(\bar{b})$. In the LHCb conventions d_i = +1(-1) if the tagged meson contains a $\bar{b}(b)$ quark.

Chapter 3

Test of the flavour-tagging algorithms

In this Chapter the main features of the three flavour-tagging algorithms used in the work are presented. Before applying them to data, many tests on Montecarlo simulations have been made to verify their correct behavior. In particular the tests focused on:

- Verifing the "calibration" of the taggers
- Determining their tagging efficiency, ϵ_{tag}, and mistag fraction ω.

3.1 Calibration check using the $B_s^0 \to D_s^{*-}\pi^+$ decays

In Figure 3.1a, 3.2a and 3.3a the decisions of the three taggers are shown. It's useful to remember that, if the decision $d = +1$, the reconstructed B meson containes a $\bar{b}-$quark, whereas if the the decision is d = -1 it contains a $b-$quark. The case with $d = 0$ corresponds to an untagged B meson. Looking at the three plots, some considerations can be made. First of all, it's easy to notice that the number of untagged mesons is the highest for the OS and the lowest for the combined tagger. Hence, the combined algorithm seems to take the best features of the OS and SS taggers. Nevertheless, these considerations aren't strong enough to consider the combined algorithm as the best one. An important fact that must be taken into account is that an algorithm could tag a $b-$quark meson as a $\bar{b}-$quark meson and viceversa, giving a wrong tag decision. So, it's necessary to evaluate the mistagging probability η associated to each tagger. This is done by evaluating the number of right and wrong tagged mesons. As in the simulations each particle is associated to an identification number, which follows the same sign-convention of the tagger decision, it's possible evaluate the number of right and wrong tag decision. In Table 3.1 the different combinations are listed.

Meson	**Particle ID**	**Tagger decision**	**Tag**
B_s^0	+531	+1	Right
B_s^0	+531	-1	Wrong
$\bar{B_s^0}$	-531	-1	Right
$\bar{B_s^0}$	-531	+1	Wrong

Table 3.1: Different possible combinations between the particle ID and the tagger decision for B_s^0 and $\bar{B_s^0}$ mesons and final tagging results.

A "calibration" plot was realized for each tagger: on the x and on the y axis the mistagging probability η and the ω function, as defined in equation 2.2, are plotted respectively. The mistagging probability can assume values between 0.0 and 0.5: the first corresponds to a perfectly correct tag, whereas the second one corresponds to a completely random tag. One expects an approximate linear dependece between the two quantities [2]. In order to verify this hypothesis, a linear fit was made. Fit results can be seen in Figure 3.1b, 3.2b and 3.3b. The linear dependence is satisfied at least in first approximation.

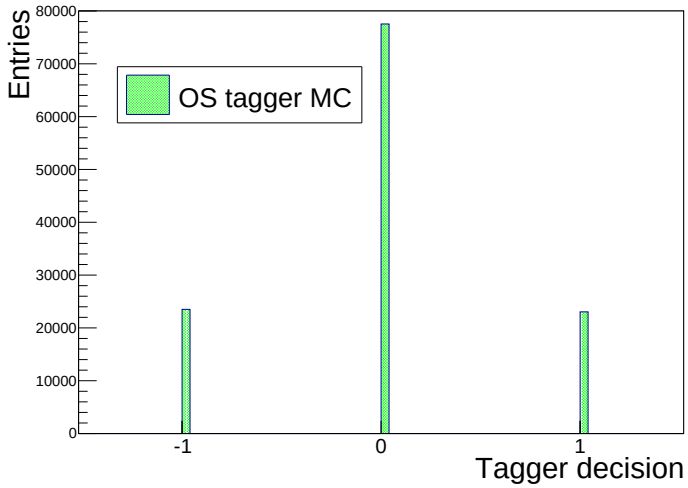

(a)

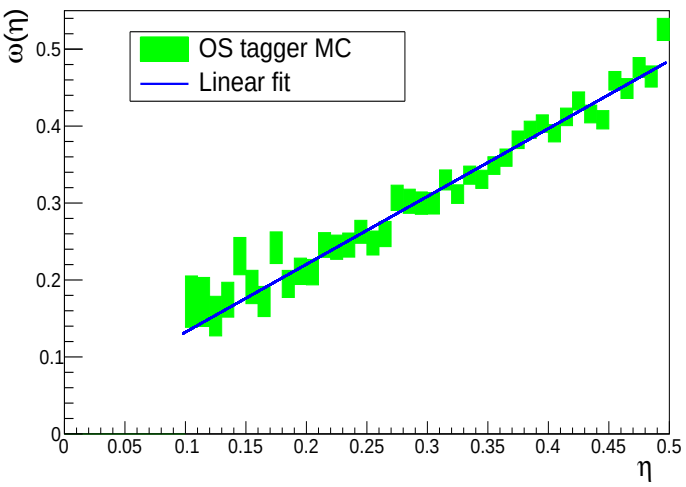

(b)

Figure 3.1: Figure (a) shows the *OS tagger* decision plot; figure (b) shows the *OS tagger* calibration curve.

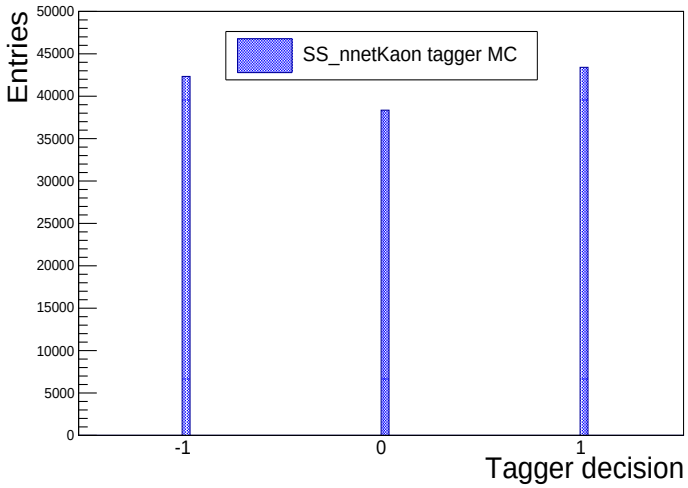

(a)

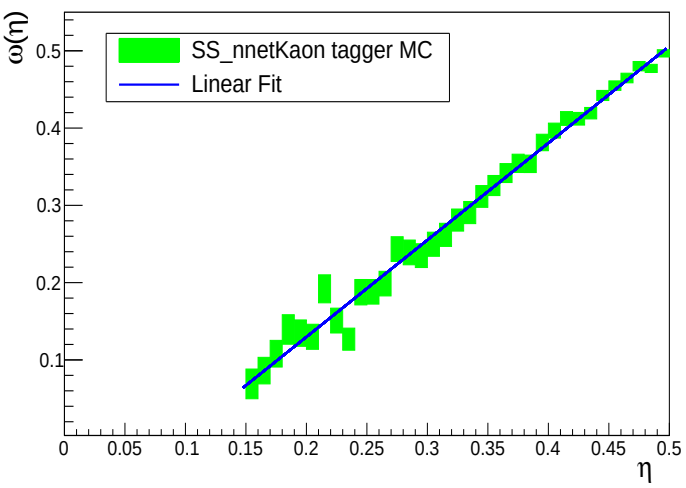

(b)

Figure 3.2: Figure (a) shows the *SSnnetKaon tagger* decision plot; figure (b) shows the *SSnnetKaon tagger* calibration curve.

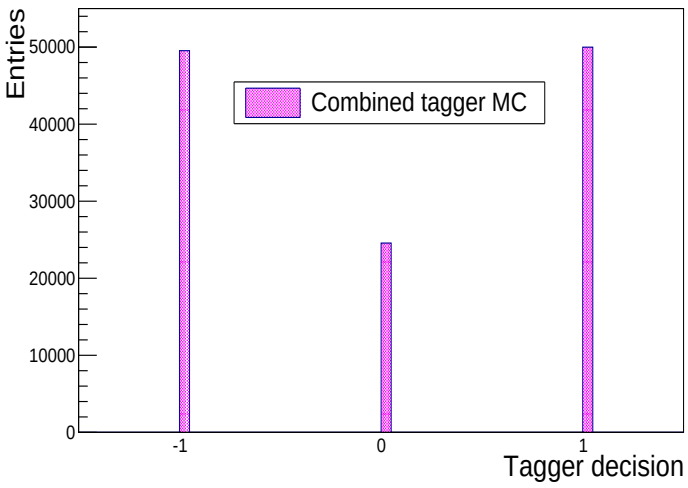

(a)

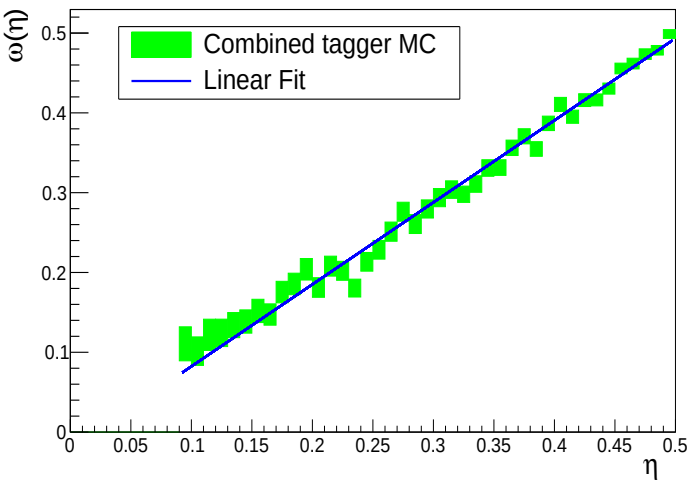

(b)

Figure 3.3: Figure (a) shows the *Combined tagger* decision plot; figure (b) shows the *Combined tagger* calibration curve.

3.2 Computation of the average mistag fraction and tagging efficiency

To complete the analysis presented in the previous section, the tagging efficiencies and the average mistag fractions were calculated. The results are shown in Table 3.2.

Tagger	ϵ_{tag}	ω
OS	0.36	0.36
SSnnetKaon	0.68	0.41
Combined	0.79	0.37

Table 3.2: Tagging efficiency and average mistag fraction for the three taggers

The average mistag fraction is about the same in each of the three cases, so the three algorithms are not so different from this point of view. A great difference can be found looking at the effectivness, ϵ_{tag}, which is the lowest for the OS and the highest for the SS+OS combined tagger. This means that the combined tagger can tag more particles than the other two taggers, without increasing the average mistag fraction.

3.3 Comparison between the $B_s^0 \to D_s^{*-}\pi^+$ and $B_s^0 \to D_s^-\pi^+$ calibrations

In Figure 3.4 the overlap of the calibration curves for the combined tagger as obtained using $D_s^{*-}\pi^+$ and $D_s^-\pi^+$ MC samples is shown. Despite the SS and OS have been calibrated on the $D_s^-\pi^+$ sample, this plot shows the portability of the taggers: it's possible to use them also on the $D_s^{*-}\pi^+$ sample.
Only the statistical uncertainty of the MC simulated sample was considered.

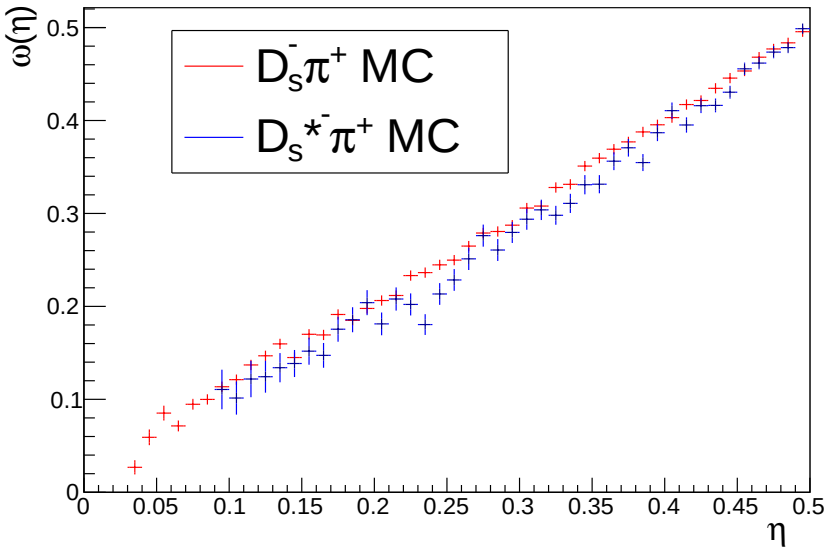

Figure 3.4: The figure shows the overlap of the $D_s^-\pi^+$ and $D_s^{*-}\pi^+$ calibration plots.

Chapter 4

Time asymmetry studies

In this Chapter the core of the work is presented. As seen in the Introduction, two different decay channels will be used to study the folded time asymmetry in B_s^0 meson decays: the $B_s^0 \to D_s^{*-}\pi^+$ and the $B_s^0 \to D_s^{*\mp}K^{\pm}$. In the following section they are both discussed and several considerations made. In this Chapter all the plots refer to the SS+OS combined tagger.

4.1 The $B_s^0 \to D_s^{*-}\pi^+$ decay channel

In MC data all variables are available at the true and at the reconstructed level. In the previous chapters, the particle ID, the tagger decision and the mistag probability variables at the reconstructed level were already described. Other important variables are:

- The lifetime of the B meson, τ
- The charge of the already mentioned "bachelor particle", i.e. the particle which accompaines the final state D_s^* meson. In the decay channel used in this section the "bachelor" particle is a charged *pion*. In Section 4.2 it will be a charged *kaon*.

It's possible to separate events given the charge of the bachelor and the particle ID or tagging information of the B meson. The different combinations are shown in Table 4.1.

Meson	Particle ID	Bachelor charge	Decay chain
B_s^0	+531	+1	$B_s^0 \to D_s^{*-}\pi^+$
B_s^0	+531	-1	$B_s^0 \to D_s^{*+}\pi^-$
$\bar{B_s^0}$	-531	-1	$\bar{B_s^0} \to D_s^{*+}\pi^-$
$\bar{B_s^0}$	-531	+1	$\bar{B_s^0} \to D_s^{*-}\pi^+$

Table 4.1: Different combinations between particle ID and bachelor charge in the $B_s^0 \to D_s^{*-}\pi^+$ decay channel.

The plots in Figure 4.1a and 4.1b correspond to the first and the fourth row of table 4.1, respectively. On the x and y axis the lifetime, τ, and the number of mesons tagged as $B_s^0(\bar{B_s^0})$ at that time are shown. The lifetime, τ, is plotted *modulo* $2\pi/\Delta m_s$, where Δm_s is a parameter characteristic of the oscillations between B_s^0-$\bar{B_s^0}$ mesons. It is set to the HFLAV [10] Fall 2014 average value. The green boxes and the points represent the MC simulation, at the reconstructed level, and the LHCb data, respectively. These corresponds approximately to 3 fb^{-1} collected in 2011-2012. Data are background-subtracted using the *sWeight* method. The $sWeight$ are extracted using the results of an invariant mass fit similar to the one shown in Figure 1.1, but performed on the $B_s^0 \to D_s^{*-}\pi^+$ sample. Making the ratio:

$$R_\pi = \frac{B_s^0 - \bar{B_s^0}}{B_s^0 + \bar{B_s^0}} \tag{4.1}$$

one obtains the so-called "asymmetry plot", where the difference, the sum and the ratio are performed at the histogram level, shown in Figure 4.3a.

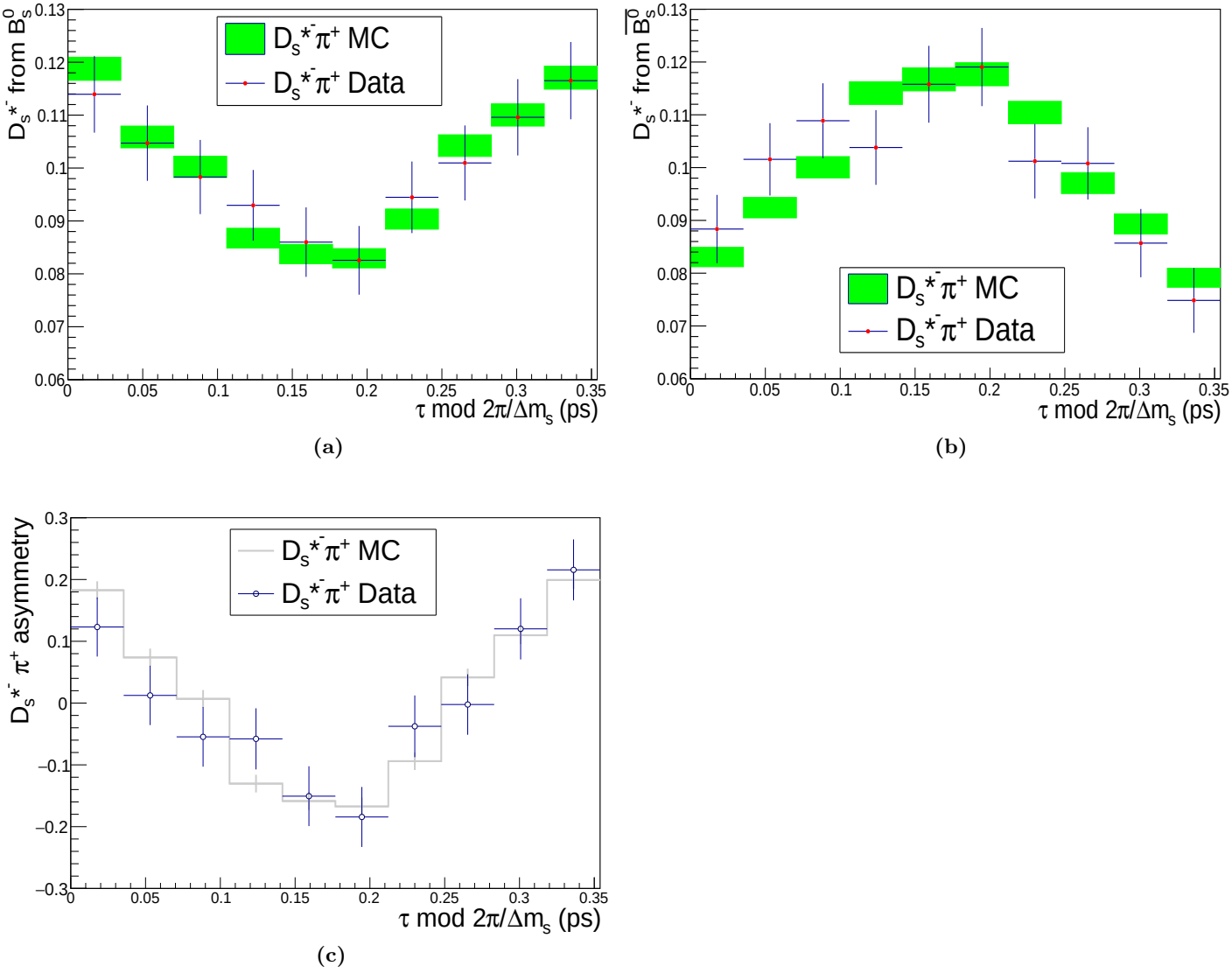

Figure 4.1: The three figures show the ovelapping of data to MC simulation. Figures (a) and (b) shows the D_s^{*-} from B_s^0 and $\bar{B}_s^0$ respectively; Figure (c) shows the $D_s^{*-}\pi^+$ asymmetry.

The previous plots correspond to "Case 4" of table 4.2. "Case 1", "Case 2" and "Case 3" refer to additional studies made on MC simulations to better understand the importance of the tagger decision. The corresponding asymmetry plots are shown in Figure 4.2a, 4.2b and 4.2c, respectively.

Lifetime τ	**Particle ID**	**Case**
True	True	1
Reconstructed	True	2
True	Tagger decision	3
Reconstructed	Tagger decision	4

Table 4.2: Different possible combinations between true/reconstructed lifetime τ and true particle ID/tagger decision.

The y axis range is set to the interval [-1,1] for each plot, in order to make comparisons easier. The different combinations produce significant differences in the amplitued of the asymmetry plot. In Figure 4.2a the maximimun (minimum) is closed to 1(-1): this is expected because the plot shows the MC simulation at the true level. The amplitude changes significantly if the tag decision is taken into account: the maximun (minimum) goes down to a value of ≈ 0.2 (-0.2). This happens when using both the true (c) and the reconstructed (d) lifetime τ. The differences are less strong if the true particle ID is combined

with the reconstructed lifetime τ (b). So the decision of the tagger is the most sensitive variable in these studies. This fact can be also probed if the plot in Figure 4.2e is considered, in which only tagger decisions with $\eta < 0.2$ are taken into account. The amplitude is larger than in Figure 4.2d with no restriction on η.

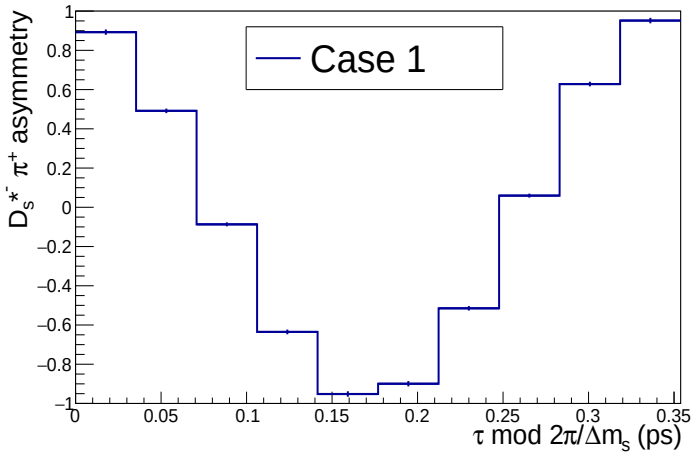

(a)

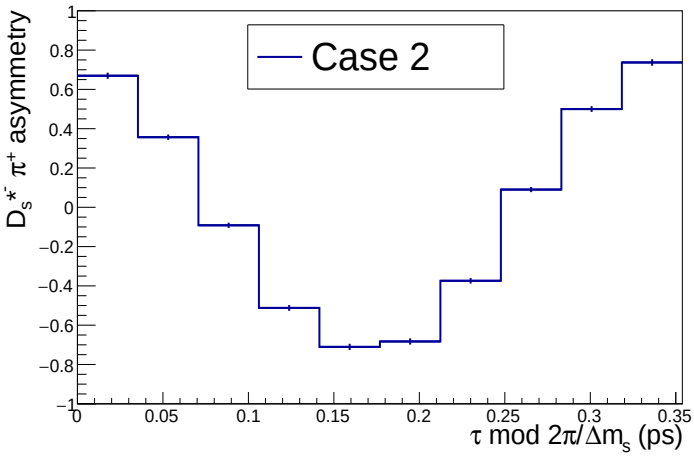

(b)

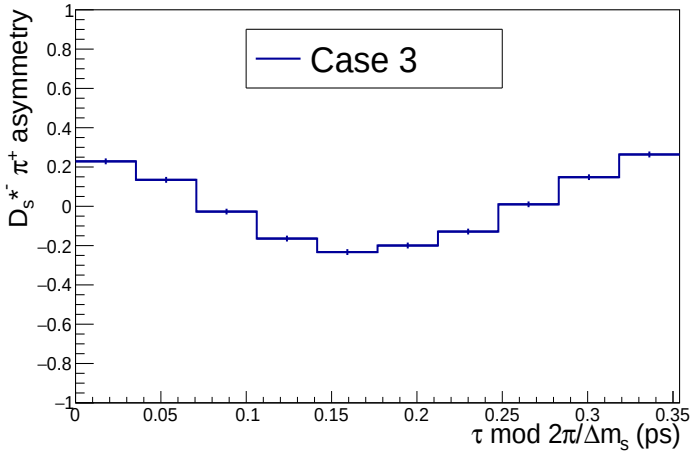

(c)

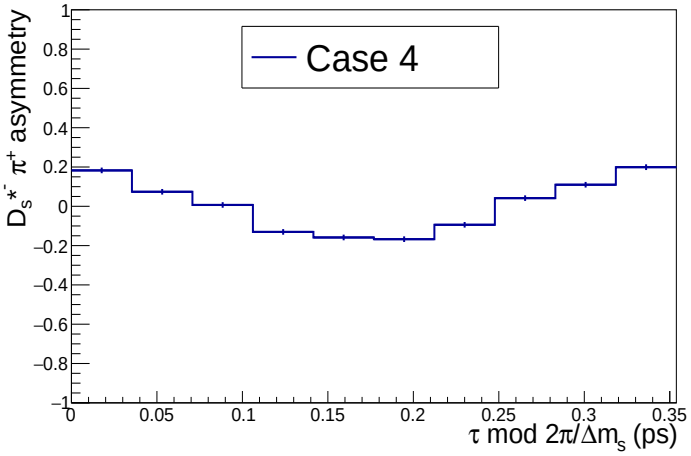

(d)

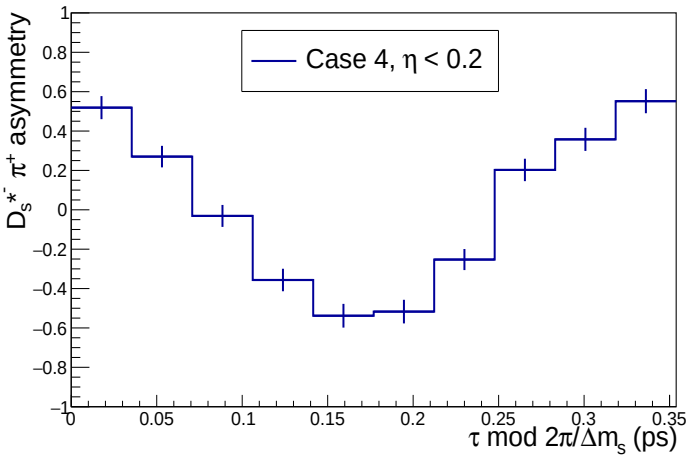

(e)

Figure 4.2: The five figures show five different asymmetry plots for the $D_s^{*-}\pi^+$ decay channel (cfr. Table 4.2). Figures (a), (b), (c) and (d) show "Case 1", "Case 2", "Case 3" and "Case 4", respectively; figure (e) shows "Case 4" with $\eta < 0.2$.

In Figure 4.3a and 4.3b the already seen $D_s^{*-}\pi^+$ and the $D_s^{*+}\pi^-$ asymmetry plots are shown, respectively. The phase difference of π at $t = 0$ shows that no CP violation is involved in this decay channel. A final check was performed: in Figure 4.4a and 4.4b the $D_s^{*-}\pi^+$ and $D_s^{*+}\pi^-$ asymmetry plots for events with $m_{B_s^0} > 5500$ MeV/c^2 are shown, respectively. No strong oscillation pattern can be seen. This fact is in good agreement with the expected "flat" behaviour using random combination of D_s, γ and π.

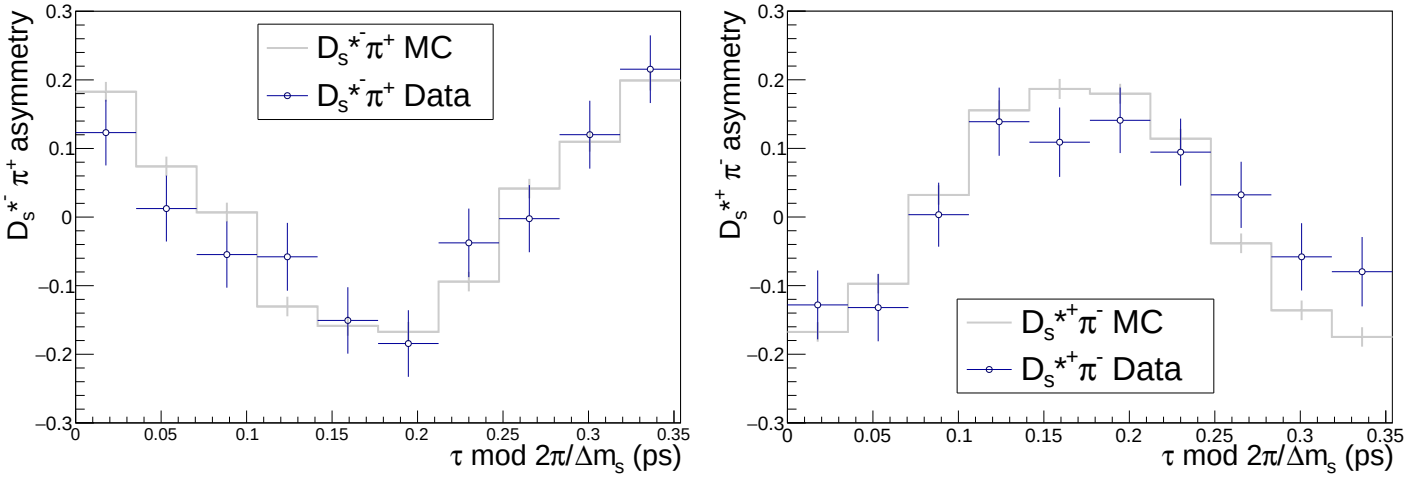

(a) **(b)**

Figure 4.3: The two figures show the ovelapping of data to MC simulation. Figure (a) shows the $D_s^{*-}\pi^+$ asymmetry plot; figure (b) shows the $D_s^{*+}\pi^-$ asymmetry plot.

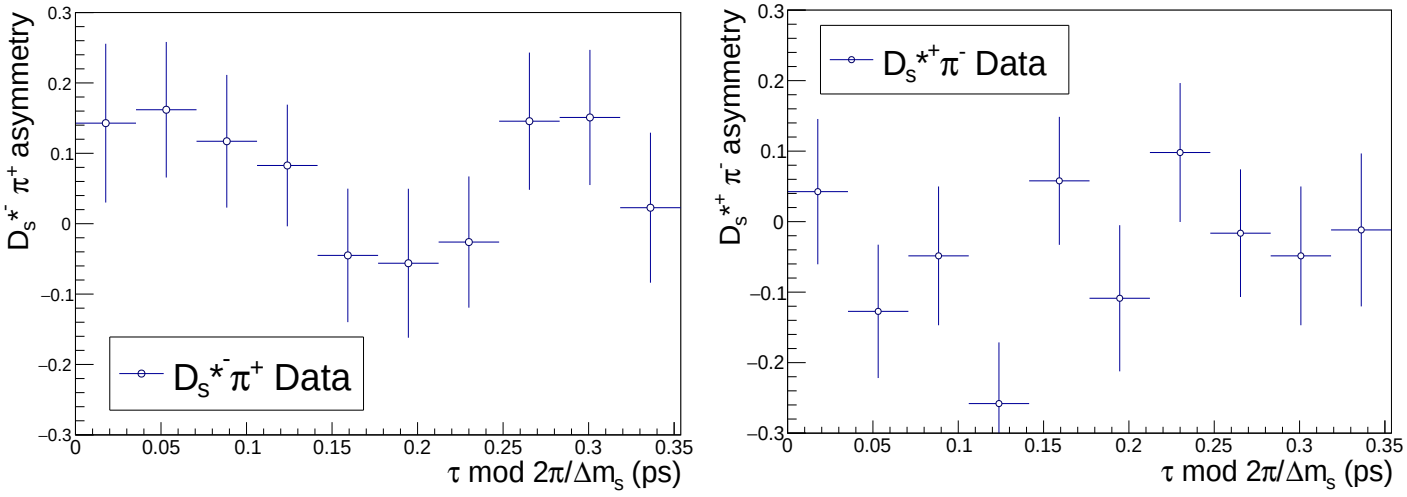

(a) **(b)**

Figure 4.4: Figures (a) and (b) show the $D_s^{*-}\pi^+$ and $D_s^{*+}\pi^-$ asymmetry plots for events with $m_{B_s^0} > 5500$ MeV/c^2.

4.2 The $B_s^0 \to D_s^{*\mp} K^\pm$ decay channel

The studies made for the $B_s^0 \to D_s^{*-}\pi^+$ decay channel have been repeated also for the $B_s^0 \to D_s^{*\mp} K^\pm$ one. Two samples of MC data were used: the first generated with no CP violation, the second with γ set to the HFLAV [10] Fall 2014 average value of 1.2776 radiants. In Figure 4.5a-4.5b and 4.6a-4.6b the asymmetry plots are shown. Now, the importance of the already discussed phase difference ϕ at $t = 0$ can be better understood: if no CP violation is involved $\phi = \pi$, whereas in any other case $\phi \neq \pi$.
In Figure 4.7a and 4.7b the overlap of $D_s^{*-}K^+$ and $D_s^{*+}K^-$ blinded data and MC simulations is shown. The data are blinded by adding two different random and unknown phases when building the data asymmetry plots of Figure 4.7a and 4.7b. Due to the smaller number of signal events in the $D_s^* K$ case with respect to the $D_s^*\pi$ one, the oscillations are not too visible. In 2015 and 2016 LHCb collected new $D_s^{*\mp} K^\pm$ data, shown in Figure 4.8a. So the same analysys could be extended to the new sample of data, giving a more clear $B_s^0 \to D_s^{*\mp} K^\pm$ oscillation pattern.

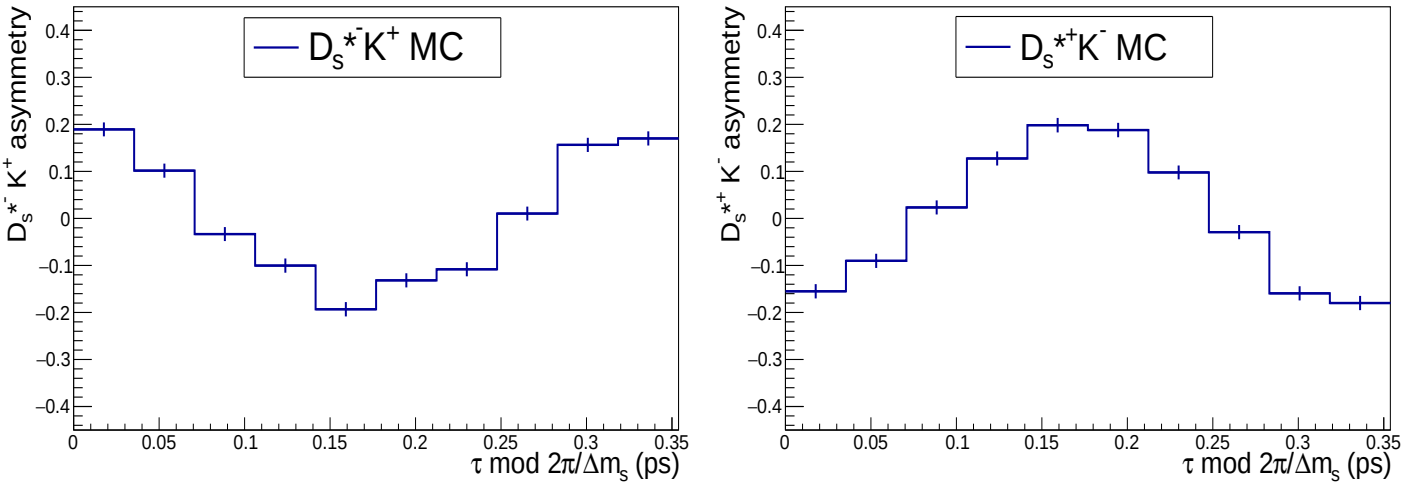

(a) **(b)**

Figure 4.5: Figures (a) and (b) show the MC $D_s^{*-}K^+$ and $D_s^{*+}K^-$ asymmetry respectively in the case of no CP violation at the generator level.

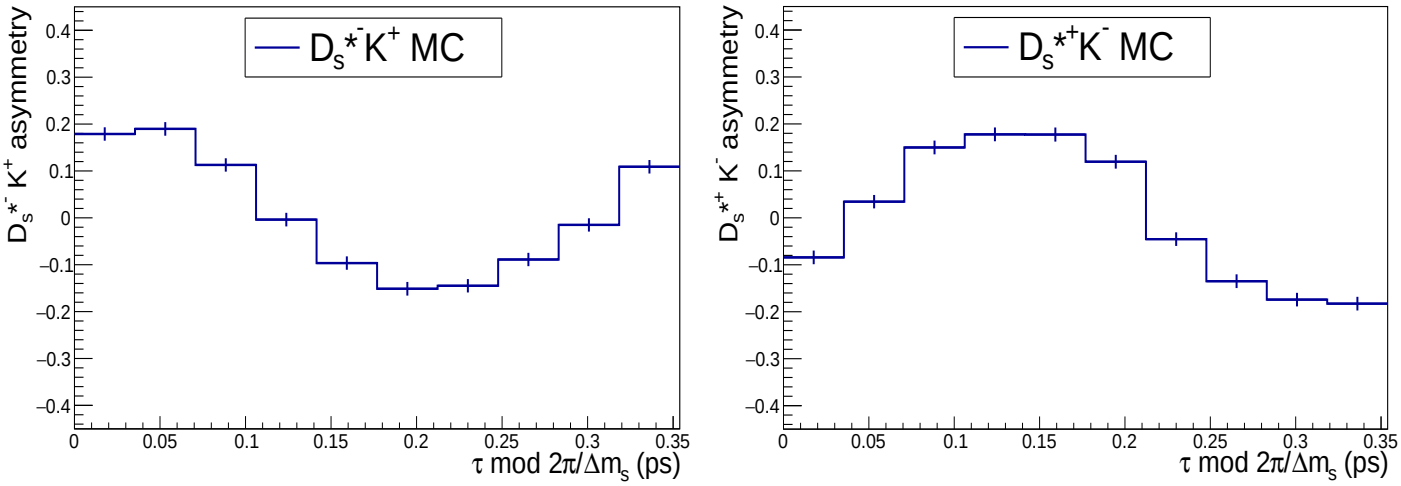

(a) **(b)**

Figure 4.6: Figures (a) and (b) show the MC $D_s^{*-}K^+$ and $D_s^{*+}K^-$ asymmetry plots respectively in the case of presence of CP violation at the generator level.

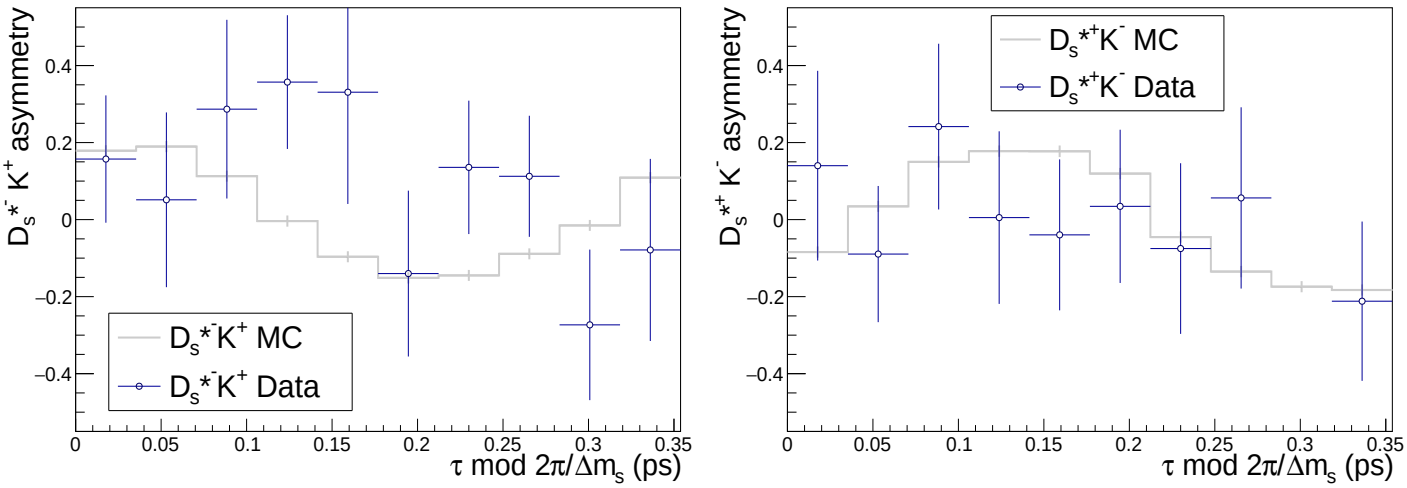

(a) (b)

Figure 4.7: Figures (a) and (b) show the overlap of the $D_s^{*-}K^+$ and $D_s^{*+}K^-$ blinded data to the corresponding MC simulation obtained in the case of presence of CP violation at the generator level.

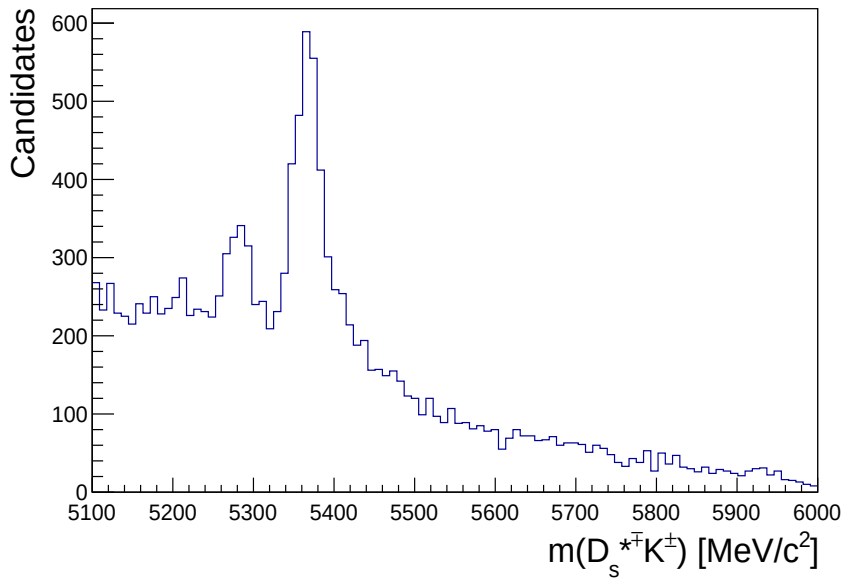

Figure 4.8: Invariant mass of the B_s^0 mesons in the $D_s^{*\mp}K^{\pm}$ decay channel. The Figure refers to 2015-2016 data collected by LHCb.

Chapter 5

Conclusions

In this work, two kind of flavour-tagging algorithms and the LHCb standard procedure to combine them were presented. A calibration test was made and the tagging efficiency, ϵ_{tag}, and average mistag fraction, ω, were calcuted, resulting in a greater tagging efficiency for the SS+OS combined tagger with no significant increase of the latter. A comparison between the calibration of the combined tagger as obtained from $B_s^0 \to D_s^{*-}\pi^+$ and $B_s^0 \to D_s^-\pi^+$ MC events was shown to probe the portability of the taggers.
Several studies were made on $B_s^0 \to D_s^{*-}\pi^+$ MC and data. Folded time asymmetry plots were built. Due to the large amount of data the flavour-oscillations were clearly visible. Furthermore, it was found that no obvious CP violation is involved in this decay channel.
In the last part of the work, the same studies were made on the $B_s^0 \to D_s^{*\mp}K^\pm$ MC and data. Due to the smaller amount of data ($\mathcal{R}^* = 0.068 \pm 0.005\ ^{+0.003}_{-0.002}$) the flavour-oscillations were not so visible. Since γ has't yet been measured in this decay channel, only the blinded data were presented.
To conclude, the histogram of the invariant mass of the B_s^0 mesons, in the $D_s^{*\mp}K^\pm$ mode, was built with the 2015 and 2016 LHCb data. A significat increase in statistic is expected when the 2011-2016 data sample will be analysed alltogether.

List of Figures

List of Tables

References

[1] LHCb collaboration, R. Aaji *et al., Opposite-side flavour tagging of B mesons at the LHCb experiment*, 2012, [**arXiv:1202.4979v2**]. Submitted to Eur. Phys. J.C.

[2] LHCb collaboration, R. Aaji *et al.,A new algorithm for identifying the flavour of* B_s^0 *mesons at LHCb*, 2016, [**arXiv:1602.07252v1**]. Submitted to J.Instrum.

[3] LHCb collaboration, R. Aaji *et al.,First observation and measurement of the branching fraction for the decay* $B_s^0 \to D_s^{*\pm} K^{\mp}$, JHEP **06** (2015) 130 [**arXiv:1503.09086**].

[4] LHCb collaboration, A. A. Alves Jr. *et al.,The LHCb Detector at the LHC*, JNIST **3** (2008) S08005.

[5] LHCb collaboration, R. Aaji *et al.,LHCb detector performance, Int. J. Mod. Phys.* **A 30** (2015) 1530022 [**arXiv:1412.6352**].

[6] LHCb collaboration, *Determination of the branching fractions of* $B_s^0 \to D_s^{\mp} K^{\pm}$ *and* $B^0 \to D_s^- K^+$, JHEP **05** 019, 2014, [**arXiv:1412.7654**].

[7] N.Cabibbo, *Unitary symmetry and leptonic decays,* Phys. Rev. Lett **10** (1963) 531.

[8] M.Kobayashi and T.Maskawa, *CP violation in the Renormalizable Theory of Weak Interaction,* Prog. Theor. Phys. **49** (1973) 652.

[9] R.Fleischer, *New strategies to obtain insights into CP violation through* $B_{(s)} \to D_{(s)}^{\pm} K^{\mp}$, $D_{(s)}^{*\pm} K^{\mp}$, *... and* $B_{(d)} \to D^{\pm}\pi^{\mp}$, $D^{*\pm}\pi^{\mp}$, *... decays*, Nucl. Phys. *B671* (2003) 459, [**arXiv:hep-ph/0304027**].

[10] Heavy Flavour Averaging Group, *http://www.slac.stanford.edu/xorg/hfag* .